The corrosion process of sterling silver exposed to a Na_2S solution : monitoring and characterizing the complex surface evolution using a multi-analytical approach

The corrosion process of sterling silver exposed to a Na_2S solution: monitoring and characterizing the complex surface evolution using a multi-analytical approach

Olivier Schalm[a*], Amandine Crabbé[e], Patrick Storme[a], Rita Wiesinger[b], Arianna Gambirasi[c], Eva Grieten[d], Pieter Tack[f], Stephen Bauters[f], Christoph Kleber[b,g], Monica Favaro[c], Dominique Schryvers[d], Laszlo Vincze[f], Herman Terryn[e], Alessandro Patelli[h]

a. Conservation Studies, University of Antwerp, Blindestraat 9, B-2000 Antwerp, Belgium
b. Institute of Science and Technology in Art, Academy of Fine Arts Vienna, Schillerplatz 3, 1010 Vienna, Austria
c. Istituto per l'Energetica e le Interfasi, Corso Stati Uniti, 4 - 35127 Padova, Italy
d. EMAT, Department of Physics, University of Antwerp, Groenenborgerlaan 171, 2020 Antwerp, Belgium
e. Research Group of Electrochemical and Surface Engineering, Vrije Universiteit Brussel (VUB), Pleinlaan 2, B-1050 Brussels, Belgium
f. XMI, Department of Analytical Chemistry, Ghent University, 9000 Ghent, Belgium
g. Centre for Electrochemical Surface Technology, Viktor-Kaplan-Strasse 2, 2700 Wr. Neustadt, Austria
h. Department of Physics and Astronomy, Padova University, via Marzolo 8, 35122 Padova, Italy

* Corresponding author
University of Antwerp
Conservation Studies
Blindestraat 9
B-2000, Antwerp, Belgium
Phone: +32 (0)3 213 71 34
olivier.schalm@uantwerpen.be

Keywords: Sterling silver, corrosion layer, evolution, Na_2S solution,

Abstract
Many historical 'silver' objects are composed of sterling silver, a silver alloy containing small amounts of copper. Besides the dramatic impact of copper on the corrosion process, the chemical composition of the corrosion layer evolves continuously. The evolution of the surface during the exposure to a Na_2S solution was monitored by means of visual observation at macroscopic level, chemical analysis at microscopic level and analysis at the nanoscopic level. The corrosion process starts with the preferential oxidation of copper, forming mixtures of oxides and sulphides while voids are being created beneath the corrosion layer. Only at a later stage, the silver below the corrosion layer is consumed. This results in the formation of jalpaite and at a later stage of acanthite. The acanthite is found inside the corrosion layer at the boundaries of jalpaite grains and as individual grains between the jalpaite grains but also as a thin film on top of the corrosion layer. The corrosion process could be described as a sequence of 5 subsequent surface states with transitions between these states.

1. Introduction

Many historical 'silver' objects are not made from pure silver (Ag999) but from silver alloyed with small but variable copper amounts [1-3]. Sterling silver (Ag925) is a commonly used alloy and is composed of 92.5 w% Ag and 7.5 w% Cu. The microstructure of Ag925 consists of an Ag-rich matrix in which a small fraction of the copper is dissolved. In this matrix, a Cu-rich phase is distributed as spheroidal inclusions of about 1 µm large [3]. The majority of silver objects have been made in a similar alloy. Therefore, Ag925 can be considered as representative for historic alloyed objects made in silver. Variations in microstructure do occur because it is not only dependent of the average composition but also from the cooling rate after casting or annealing. Low-grade alloys (e.g. 80 w% Ag and 20 w% Cu) or silvered objects are not targeted in this study.

Over time, the white and shiny surfaces of silver alloys are lost due to the formation of a corrosion layer. The driving force behind this corrosion process are hydrogen sulphide (H_2S) and carbonyl sulphide (OCS) with typical indoor concentrations of 0.086 ppb – 0.6 ppb and 0.4 ppb – 0.85 ppb respectively [4-7]. No matter the composition of the silver alloy, all fully developed tarnish layers have the same visual appearance: black and dull. For many heritage objects such as jewellery, liturgical attributes or photographic media, such tarnish films are considered as aesthetically displeasing and can obscure the readability of for example silver-based photographic materials.

The corrosion process of pure silver in different kinds of environments is widely studied: (1) ambient conditions [6,8], (2) synthetic air containing moisture and small concentration of reactive gases such as H_2S, OCS, SO_2, CO_2 and/or O_3 [9-15], or (3) alkaline Na_2S solutions [16,17]. However, these studies of the corrosion mechanism of pure silver in different kinds of environments can hardly be considered as representative for objects made from silver alloys. For Ag925, it is known that the corrosion rate is higher when compared to pure silver [18] while the Cu-rich phase in the alloy is preferentially attacked by H_2S [3,19]. This results in Cu-rich (e.g., cuprite, tenorite, digenite), Ag-rich (e.g., acanthite, argentite, chloro-argyrite, silver oxide) , and even in Cu,Ag-mixed (e.g., stromeyerite) corrosion products [20-26]. In a previous investigation, polished Ag925 coupons are exposed to two different uncontrolled indoor environments for a period of 6 months [27]. The X-ray spectra collected with scanning electron microscopy from these early corrosion states demonstrated the presence of oxides and not of sulphides as was originally expected. This suggests that the chemical composition of the corrosion layer is not constant and that it evolves as corrosion proceeds. For the alloy Ag925, the role of small copper amounts on the corrosion process will be studied, as well as how composition, chemical speciation and microstructure of the corrosion layer evolves over time.

2. Experimental

2.1. Sample preparation

Coupons (20 mm x 50 mm) are cut from larger sheets of Ag925 (Schöne Metals Corporation, Degussa, Germany) using a parallel metal cutting guillotine. This methodology ensures coupons with identical microstructural properties (i.e. with an analogue distribution and surface area ratio of Cu-rich inclusions in the Ag-rich matrix.). The front side is grinded and polished with a fixed procedure to obtain as close as possible identical surface states. On the surface of the coupon, a small amount of water soluble polishing pastes (3M™ Finesse-it™ Finishing Material, followed by 3M™ Imperial™ Machine Glaze) is applied and the surface is brought into contact with a soft cotton rotating wheel for approximately 1 minute. Cleaning of the polished surface is performed by immersing the coupon in an ultrasonic bath with ethanol for 2 minutes. Afterwards, the coupons are rinsed with deionised water and dried with oil- and water-free compressed air. The mirror-like appearance of the surface is very similar to that of historical 'silver' objects finished with a traditional mechanical and abrasive polishing technique [28-30].

2.2. Corrosion method

The Ag925 coupons are exposed to subsequent cycles consisting of a short immersion (12 s for every cycle of 60 s) of the coupon in a Na_2S solution (0.1 mol/L $Na_2S.9H_2O$, pH = 14) followed by a longer exposure to air (48 s/60 s cycle) [31]. Dissolved sulphides are known to make the solutions alkaline. The corrosion procedure has been used in two different ways in order to obtain subsequent surfaces states that can be analysed with analytical techniques:

1. **Stop motion method applied to a single coupon:** A single polished coupon is exposed to the same solution for short exposure times interspersed by surface analyses. This approach has the advantage that the evolution of exact the same position at the surface can be studied.
2. **Series of coupons with various exposure times:** An alternative approach is to generate a series of coupons that are simultaneously immersed in the same Na_2S solution. The use of the same solution assures that differences between the coupons are only due to the exposure time. The exposure time in the series of coupons varied between 0 minutes to 300 minutes. The advantage of this corrosion method is that all states can be analysed without being dependent on the corrosion procedure.

2.3. Characterization of surface states

It is possible to determine how the surface of Ag925 evolves during the corrosion process by following 8 surface properties: reflectance, surface colour, topography of the surface, microstructure of the surface, microstructure of the lateral face perpendicular to the surface, oxidation state of copper, concentration of species in the corrosion layer and thickness of the corrosion layer. The surface properties are used to identify the sequence of dominant surface states within the corrosion process. The techniques used to determine these properties are grouped in three different levels.

a) Visual observation at the macroscopic level

The visual appearance of the Ag925 surface plays a crucial role in heritage science. For that reason, the evolution of colour and reflectance has been determined following the measurement methods described in the list below. In addition, microscopic observation has been included in this level, because it is often the first step in the analysis of heritage objects performed by conservation scientists.

- **Gloss meter:** The fraction of specularly reflected light (i.e., reflectance) is measured with an Elcometer 406 Novo-gloss Lite™ miniature gloss meter. Due to the high reflectance of some corrosion states, the reflectance is systematically measured at an angle of incidence of 20°.
- **UV-vis spectrophotometry and colour measurements:** UV-vis spectra are collected with an Avantes spectrophotometer consisting of an AvaLight-DH-S-Bal light source combining a halogen-tungsten lamp for IR and visible light and a deuterium lamp for UV-light in combination with an Avaspec-2048 spectrometer. Light source and detectors are coupled to a 50 mm integrating AvaSphere using fibre-optic cables. The surface is illuminated at an angle of incidence of 8°, while the diffusely reflected light is measured at 90°. This instrument is also used to determine the surface colour from 5 mm diameter zones by measuring the L*a*b*-values. The change in colour when compared to the original surface state is calculated as the Euclidean distance CIE $\Delta E'76$ [32].
- **Optical microscopy:** The microstructure of the surfaces is visualized with an Olympus DSX510 optical microscope in bright field observation. By creating a z-stack with the Extended Focal Image (EFI) function, high resolution colour images are acquired at elevated magnification. The sample stage is set to a fixed position with an L-shaped metal positioning aid to allow image collection from exactly the same location of a coupon.

b) Chemical information at the microscopic level

The next level in the characterization of the surface is performed by using (micro-) analytical techniques such as electrochemical measurements or electron microscopy. The information obtained with these techniques is supplemented with synchrotron analyses.

- **Electrochemical measurements:** Electrochemical analyses are used to perform a chemical speciation of the corrosion products present at the surface of metal coupons. The measurements are performed in a three-electrode cell in which the coupon is the working electrode and a platinum grid the counter electrode. A Saturated Mercurous Sulphate Electrode (MSE; Hg/Hg_2SO_4/saturated K_2SO_4; 0.615 V versus standard hydrogen electrode) is used as reference electrode. A $NaNO_3$ solution of 0.1 mol L^{-1} is used as electrolyte. The three-electrode cell contained a small aperture of 5 mm diameter (i.e., 0.2 cm^2) which give access to the coupon surface. Voltage or current is applied with a Palmsens3® potentiostat/galvanostat (PalmsensBV). Linear sweep voltammetry is used to reduce the tarnish layer by applying a potential between -0.6 V and -1.7 V vs. MSE at a scan rate of 2 mV s^{-1} while measuring the variation in current. It is used to identify corrosion products. With the same setup, chronopotentiometric analyses of the corrosion layers are performed by applying a constant current of -100 µA while measuring the variation in voltage over time. Transition times between two subsequent abrupt changes in potential are determined from the first derivative of the chronopotentiograms calculated with a 11-point Golay-Savitzky filter. The principle of chronopotentiometry for the reduction of surface films is described elsewhere [33]. This technique is used to determine the surface concentration of the corrosion products.
- **Electron microscopy:** The surfaces are inspected with a Field emission gun - scanning environmental electron microscope equipped with an EDAX Genesis energy dispersive X-ray detector (FEG-ESEM-EDX) FEI Quanta 200 F. The X-ray detector is equipped with a ultra-thin-window and has an energy resolution of 136 eV at Cu-Kα FWHM when using a voltage of 25 kV. The FEG-ESEM-EDX is used to collect secondary electron (SE) and backscattered electron (BSE) images with a magnification up to 50000x (lateral resolution: 30 nm). Simultaneously, FEG-ESEM-EDX is used to perform chemical analyses by collecting X-ray spectra and X-ray maps at a voltage of 20 kV. All measurements have been performed below a maximum electron density in order to avoid reductive changes of Ag_2S [34]. For 20 keV electrons, the Kanaya-Okayama equation gives a penetration depth of about 1.4 µm in pure silver. The depth of information for backscattered electrons is approximately 0.22 times the Kanaya-Okayama range which is about 300 nm [35]. According to the Anderson-Hasler equation [36], the X-ray ranges and corresponding information depth for the S-Kα and Ag-Lα lines in Ag_2S are both about 1.3 µm. In addition to the surface analyses, also cross-sections are investigated by analysing the lateral faces of a cross-cut. The cross-cuts of a size of about 30 µm x 10 µm are created in the surface by means of a FEI Quanta 200 3D FIB/SEM using Ga^+ bombardment. Besides the ion milling module, the system is also equipped with detectors for secondary and backscattered electrons and an energy dispersive X-ray detector with which the lateral faces of the cross-cut can be analysed.
- **X-ray absorption near edge structure (XANES):** The oxidation state of copper close to the surface of corroded Ag925 coupons is determined by XAFS measurement performed at the DUBBLE EXAFS beamline (BM26A) of the ESRF facility (Grenoble, France) using an experimental setup described elsewhere [37]. The coupons are measured in fluorescence mode under grazing exit geometry (Entrance angle: 43°; Exit angle: c. 2°) in order to reduce self-absorption effects and to obtain information mainly from the surface layer. In this measuring geometry, the information depth of Cu-Kα X-ray photons is approximately 1 µm. The incident beam is focussed using a polycapillary optic where the focal beam size is dependent on the energy (c. 24 µm at 9 keV) while the fluorescence signal is detected using a Vortex-EM SDD detector. Reference materials are Cu-foil and pellets made from pure product powders obtained at the company Alfa Aesar (CuO, Cu_2O, CuS, Cu_2S) and diluted in cellulose. The complete XAFS spectra are fitted by a linear combination

of reference spectra in order to determine the ratio of species present in the corrosion layer. This is performed with software developed by the XMI research group.

- **X-ray diffraction:** XRD analysis was performed on non-oriented powder samples using a Philips X'pert System (Cu Kα radiation, scan time 1 s per 0.02° 2-theta). The powder was obtained by corroding the same Ag925 plate in cycles of 8 hours interspersed by mechanical collecting corrosion from the surface.

c) Information at the nanoscopic level

For a specific surface state from the Ag925 series (i.e., coupon with an exposure time of 60 minutes) in-depth information at the nm-level is obtained. For this characterization, the following analytical methods are used:

- **Synchrotron - X-ray photoelectron spectrometry (SR-XPS):** The surface characterization at the nm-level is performed by synchrotron - X-ray photoelectron spectrometry (SR-XPS). For this, the instrument installed at the end station at the NanoESCA beamline of the Elettra storage ring (Trieste, Italy) combines an electrostatic Photo Electron Emission Microscope (PEEM) with a double-hemispherical ('IDEA') analyser. The fast overview and high-resolution narrow spectra for Cu3p, Cl2p, S2p, C1s, Ag3d are collected using a soft X-ray source of 450 eV. The spectra are calibrated using the Fermi cut-off in the valence band spectra.
- **Transmission electron microscopy (TEM):** A thin lamella perpendicular to the sample surface is removed from the coupon by FIB. This is done in accordance with the wedge-cut method followed by an in situ lift out technique [38]. In order to preserve the morphology of the surface, the sample is first covered with a Pt layer, which is obtained by ion beam assisted deposition. The lamella is generated using dual beam FIB/SEM (FEI Helios Nanolab TM650) with a Ga^+ source for thinning. The lamella is thinned using a Ga^+ ion applied at a series of decreasing voltages and currents and with a final cleaning at 2kV and a low current of about 1 µA. For the characterization of the inner structure of the corrosion layer at a nm-level, analyses are performed with a FEI Osiris transmission electron microscope (TEM) equipped with a four-quadrant, windowless EDX detector. It is used to collect conventional TEM images, High-Angle Annular Dark Field – Scanning Transmission Electron Images (HAADF-STEM) images and EDX spectra. The instrument is operated at 200 kV. To distinguish the jalpaite (Ag_3CuS_2) from acanthite (Ag_2S) and chalcocite (Cu_2S), the TEM analyses are performed under cooling conditions to ensure the jalpaite has a distinguishable tetragonal structure [39].

3. Results

In the first paragraph, the visual observation methods will be used to observe the evolution of a single tarnishing Ag925 coupon enduring the stop motion corrosion method (i.e., corrosion method 1 in paragraph 2.2). In the following paragraph, the series of Ag925 with various exposure times (i.e. corrosion method 2 in paragraph 2.2) will be used to extract chemical information at the µm-level. In the last paragraph, the in depth analysis of the corrosion state obtained after 60 minutes of exposure will be given. This corrosion state is studied in detail because the surface contains a well-developed grey tarnish layer that is well attached to the substrate.

3.1. Visual observation at the macroscopic level obtained from the stop motion method

The evolution of the visual appearance of an Ag925 coupon is monitored by measuring the average colour and reflectance. In Fig. 1a, the reflectance drops very rapidly in the early stage of the corrosion process, then the reflectance restores to some extent whereupon it slowly decreases again. The colour evolution is shown in Fig. 1b. Visually, first the coupons surface turns yellow, then it becomes blue and finally it becomes grey.

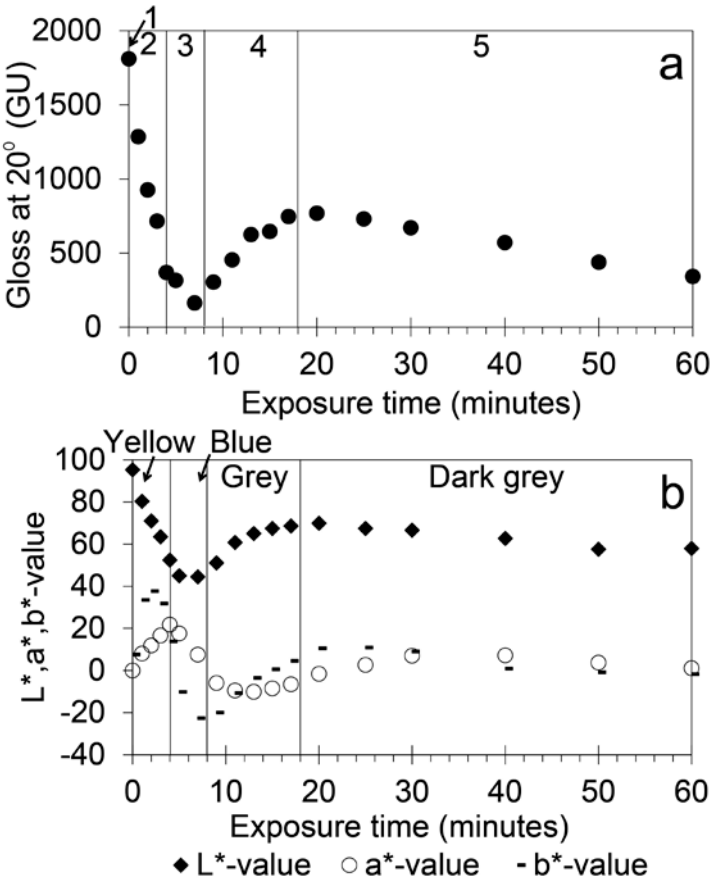

Fig. 1: Evolution of reflectance and colour as the stop motion corrosion method proceeds. The transition between the most remarkable surface states are visualized by vertical lines and the surface states have been numbered. a) Reflectance at 20° as a function of exposure time; b) L*a*b*-values as a function of exposure time.

For the sake of clarity, a small detail (22 µm x 22 µm) is shown in Fig. 2 of the complete area (124 µm x 124 µm). The larger images are reported elsewhere [40]. The collected images clearly demonstrate that corrosion starts at specific surface locations. There, first a white spot surrounded by a blue ring is formed and only later a grey centre in the middle of the white spot is seen. While these areas appear to expand over the surface, new spots are being formed. Meanwhile, the surface between the spots changes in colour from yellow over blue to grey. The colour between the spots seems to correspond with the colour measured at mm-level which is given in Fig. 1b. From the analysis of reflectance, colour and growth of the spots, 5 dominating surface states could be identified. They are described in the list below:

- **Surface state 1 with mirror-like appearance (Fig. 2, 0 minutes):** The dark spots visible on the freshly white and mirror-like polished surface correspond with the Cu-rich inclusions. These small inclusions have a limited impact on the final colour of the polished coupon. Some larger discoloured zones can be seen. They correspond with the locations where the first spots (i.e., after 1 minute of exposure) will be formed.
- **Surface state 2 with yellow appearance (Fig. 2, exposure time up to 3-4 minutes):** The surface contains isolated spots that are considerably larger than the original Cu-rich inclusions visible on the polished metal. The white spots have a grey centre and blue ring. As corrosion proceeds, existing spots expand and new spots are formed. The increasing amount of isolated spots results in enhanced surface roughness, explaining the drop in reflectance seen in Fig. 2a. The zones between the spots become yellow, which is the visually dominating colour. The dominating yellow colour can be seen in Fig. 2b as an increase in the b*-value (yellow), reaching a maximum at an exposure time of 2 minutes. At the same time, there also is a slower increase in the a*-value (red), reaching a maximum at 4 minutes. This means that the yellow colour evolves to a reddish surface.

The drop in the L*-value signifies that the surface becomes darker, which coincides with a drop in the reflectance;

- **Surface state 3 with blue appearance (Fig. 2, from state 2 up to 7-9 minutes):** At longer exposure times, the surface between the spots become blue, resulting in a visually blue appearance of the coupon. This can be seen in Fig. 2b by the negative values of b* (i.e., blue) and a decrease in the a*-value (i.e., more greenish). In this state, the reflectance continues to drop until it reaches a minimum at 9 minutes of exposure.
- **Surface state 4 with grey appearance (Fig. 2, from state 3 up to 17-20 minutes):** The overall colour of the surface has a grey colour. The most remarkable change between this state and the previous one is the enhancement of the reflectance and the brightness (i.e., higher L*-values). The white zones around the grey centres merge into each other so that only the grey centres remain as isolated spots on the surface. It can be suggested that the lowered surface roughness results in higher reflectance values due to the lateral growth of crystalline corrosion products.
- **Surface state 5 with dark grey appearance (Fig. 2, from state 4 onwards):** During this state, a dark grey corrosion product is formed from the grey centres. This new corrosion product gradually covers the complete surface. This results in a dark grey coloured coupon. In this surface state, the reflectance slowly drops again while the surface colour become darker.

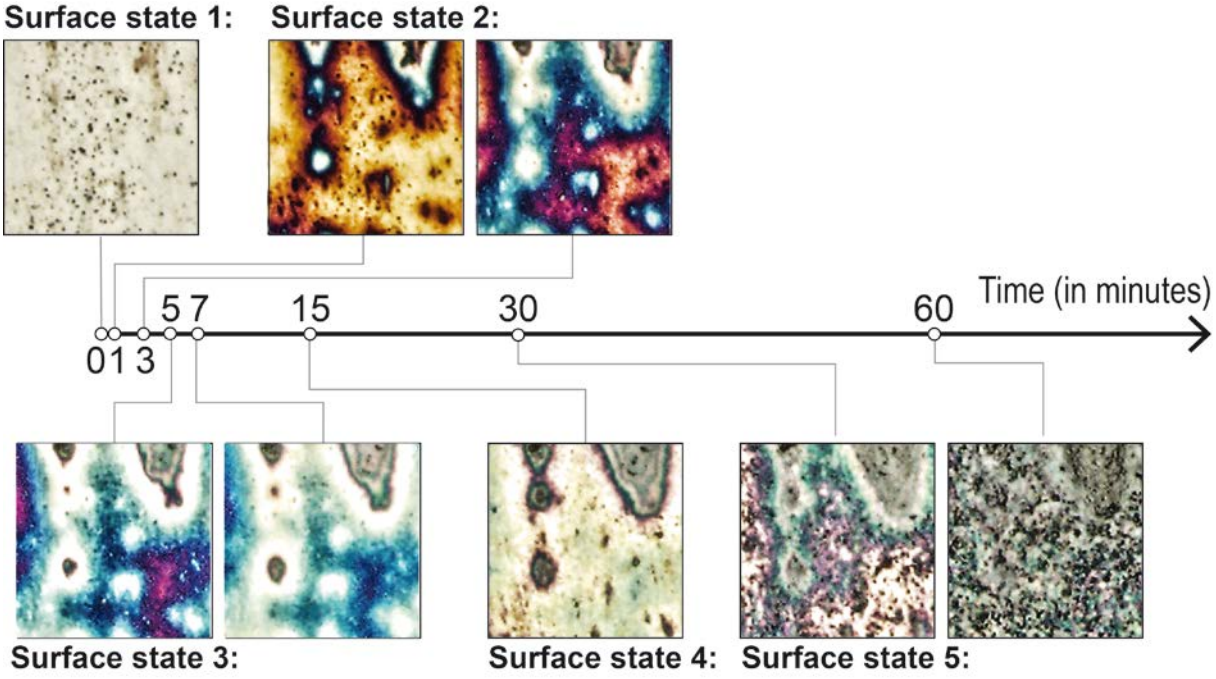

Fig. 2: Bright field images collected with the DSX510 microscope at magnification 2000x. The width of the images is 21.7 µm. The sequence of images is obtained from exactly the same position from the same Ag925 coupon that underwent the stop motion method. The timeline shows fast and drastic changes in the beginning of the corrosion process and slower changes further on. Besides the well identifiable surface states also intermediate states are shown.

3.2. Chemical information from the series of tarnished Ag925 coupons

The chemical evolution of the surface is analysed by collecting X-ray spectra with SEM-EDX from a series of coupons with various exposure times. It can be stated that the incident electrons are able to penetrate the corrosion layer completely because at 300 minutes exposure this layer has a thickness of about 1 µm (see cross section in Fig. 6) while the information depth of the S-Kα line is about 1.3 µm. When considering a corrosion layer with a constant composition and no self-absorption, the intensity of the S-Kα line must be proportional with the film thickness. Fig. 3a shows a linear relation between the S-Kα peak intensity and the square root of the exposure time. This means that the film growth is rapid at the onset of the process and tends to slow down with time. This is a typical relation for diffusion processes. However, the behaviour of Cu at the surface is much more complicated and cannot

be explained by a simple diffusion process. Fig. 3b suggests that Cu is gradually enriched until it reaches a maximum. In a later stage the Cu-content seems even to drop.

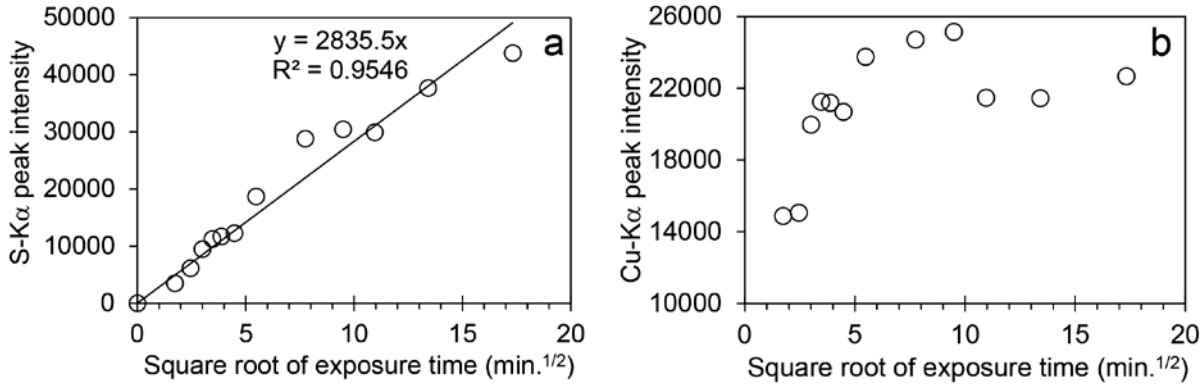

Fig. 3: Evolution of the surface composition. a) S-Kα peak area determined from the X-ray spectra collected from the surface using SEM-EDX as a function of the square root of the exposure time; b) The Cu-Kα peak area as a function of the exposure time.

More detailed information can be obtained from a chemical speciation of the corrosion layer using linear sweep voltammetry and chronopotentiometry. From the reduction of the corrosion products (Fig. 4a) it is possible to identify at least 3 different species: -0.6 V (unidentified product), -1.30 V (Ag_2S) and -1.55 V (Cu_2S) vs. MSE [41]. The freshly polished metal shows only a small peak at -0.6 V and at -1.55 V. The following information is obtained by analysing a series of Ag925 coupons with various exposure times:

- **Surface state 2, 3 and 4 (Fig. 4, up to 20 minutes):** The transition times of the corrosion products as determined by chronopotentiometry are shown in Fig. 4b. For all the surface states in the first 20 minutes, Ag_2S is not detected in the corrosion layers. This means that the yellow, blue and grey surface colours must be the result of Cu-rich corrosion products. In the voltammograms a small signal located at around -0.6 V/MSE might be due to the presence of some kind of oxide in the corrosion layer during the early stage of the corrosion process. The presence of copper oxides as initial corrosion product is also observed during the sulphidation of copper in atmospheric conditions [42,43].
- **Surface state 5 (Fig. 4, from 20 minutes onwards):** Only at longer exposure times, Ag-rich species are identified as corrosion products. This means that Cu-rich corrosion products are formed first, while Ag-rich corrosion products are formed in a later stage. In addition, the surface concentration of all corrosion products increased over time.

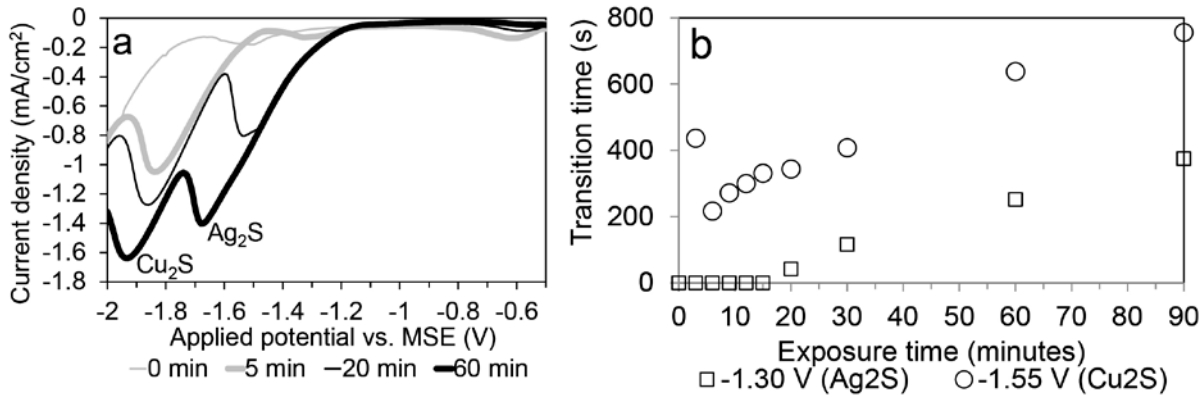

Fig. 4: Surface speciation of the Ag925 surface is performed by reducing the corrosion products in a 0.1 mole/L $NaNO_3$ solution. a) Linear sweep voltammetry of the tarnished surface as a function of exposure time; b) Transition time at specific reduction potentials (vs. MSE) as determined from chronopotentiometric analyses.

Additional information about the evolution of the surface is obtained by studying the evolution of the topography and the microstructure. The following information is obtained by means of electron microscopy:

- **Surface state 1 (Fig. 5, 0 minutes):** The surface of the polished coupon consists of a bright Ag-rich matrix containing dark Cu-rich inclusions with a size of c. 1 µm. The Cu-rich inclusions shown in the BSE image are not homogeneously distributed. The SEI images show the presence of scratches due to the polishing action.
- **Surface state 4 (Fig. 5, 9 minutes):** When corrosion forms, dark spots of about 20 µm to 30 µm large can be seen in the BSE images. The large contrast between spots and surrounding material is the result of a different mean atomic number. For the surface between these spots, the underlying Cu-rich inclusions remain visible. This means that the surface between the spots must be covered by a corrosion layer that is smaller than the information depth of backscattered electrons. Therefore, this layer must be smaller than 300 nm. The topographic contrast in the SEI images shows well defined spots that consist of platelets. They are higher in topography. Since no Ag_2S has been formed in that stage (see Fig. 4), both spots and zones between spots must consist of Cu-rich corrosion products.
- **Surface state 5 (Fig. 5, 30 minutes):** In the bright field images of Fig. 3 the isolated spots become larger while the surface between the spots evolves from yellow over blue to grey. The contrast between spots and surrounding material starts to diminish. However, in the BSE images, the spots remain clearly resolved up to this state. The surface roughness of the zone between the spots strongly increases.

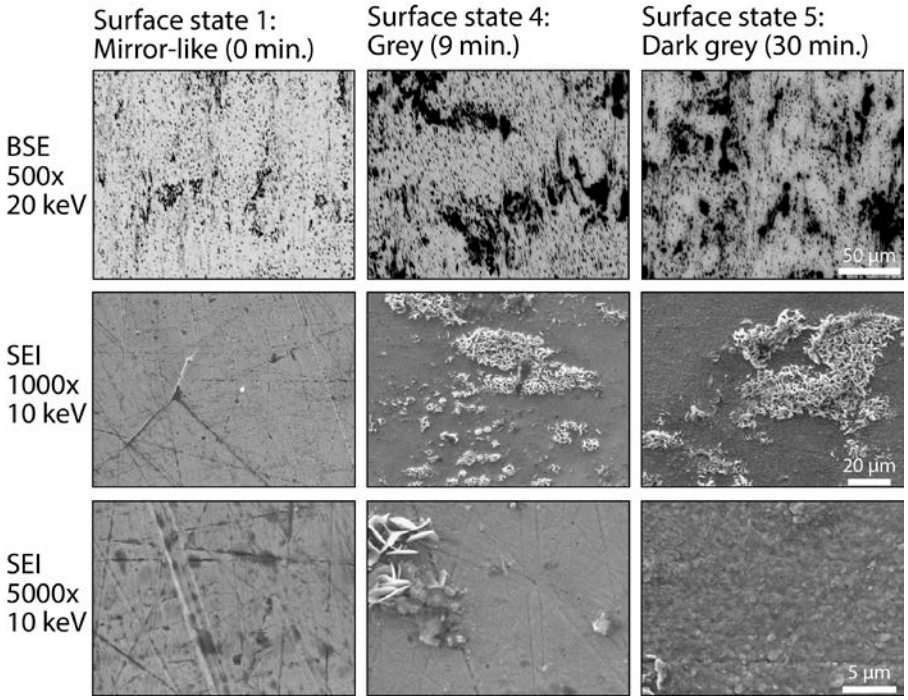

Fig. 5: SEM images collected of the surface of coupons exposed to different exposure times. The top row images give an overview of the surface. The middle row images visualizes the areas containing platelets, while the bottom row images visualizes the surface between the areas with platelets.

From the same series of coupons shown in Fig. 5, backscattered electron images are collected on the cross-cuts obtained by ion milling (Fig. 6). It allows the study of the interface between the corrosion layer and bulk material. The following information is obtained for the subsequent surface states:

- **Surface state 2 (Fig. 6, 3 minutes):** The Cu-rich inclusions of about 1 µm are somewhat darker than the brighter Ag-rich matrix. A Cu-rich inclusion is located at the surface. The surface is covered by a sulphide film with a thickness of about 50 nm.
- **Beginning of surface state 4 (Fig. 6, 9 minutes):** A void just below the surface can be seen. The shape and position of the void suggests that it is a former Cu-rich inclusion of which the copper is displaced and spread laterally over the surface as a Cu-rich corrosion product. The sulphide film has a thickness of 100 nm – 300 nm.
- **Surface state 5 (Fig. 6, 300 minutes):** The interface between the corrosion layer and bulk metal consists of large voids with a height of about 400 nm – 800 nm. It is clear that the voids do not longer follow the shape of the Cu-rich inclusions, meaning that also the silver in the Ag-rich matrix has displaced during the corrosion process. At 300 minutes of exposure, the corrosion layer with a thickness of about 1 µm is attached to the bulk by some filaments.

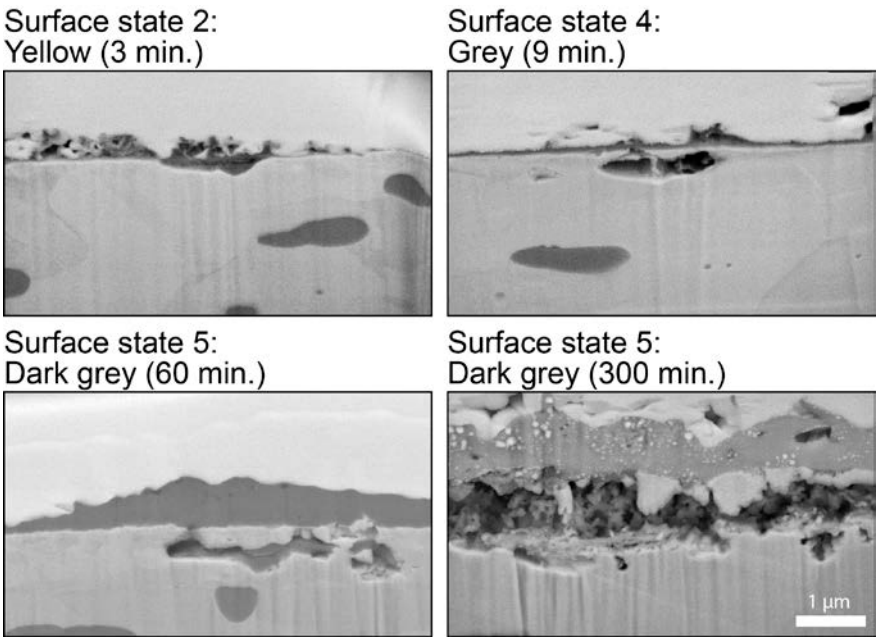

Fig. 6: Backscattered electron images of the cross-cuts obtained by ion milling and studied at a magnification of 20000x. The images show the formation of voids beneath the surface. At the bottom of the images the Ag925 alloy with darker Cu-rich inclusions and brighter Ag-rich matrix can be seen. The dark grey layer at the surface is the corrosion layer. At the top of the image, the Pt layer can be seen which is deposited during the FIB treatment.

Fig. 7a show how the XAFS spectra changes at the Cu-K edge as a function of exposure time. The linear combination fitting of these spectra resulted in a chemical speciation of the Cu compounds, which is summarized in Fig. 7b. By using the subtle differences between the Cu_2S and CuS spectra, it is possible to make a distinction between both compounds. Unfortunately, this technique did not allow the speciation of silver due to interference with the substantial amounts of Ag in the matrix below.

- **Surface state 1 (Fig. 7a, 0 minutes):** Fig. 7b shows that the polished surface contains mainly metallic copper, although small amounts of copper oxides and sulphides are present as well. The corrosion products are probably due to the natural corrosion after the surface has been polished within the period between sample preparation and analysis.
- **Surface state 2 (Fig. 7a, 1 and 3 minutes):** For the yellow coloured corrosion layer, the XAFS spectra of 1 minute and 3 minutes in Fig. 7a are clearly different. The linear combination fitting of the spectra does significantly show a contribution of copper sulphide compounds and small amounts of oxides. Copper oxide XAFS spectra have a very characteristic white line feature (which is not present for the sulphides). Therefore, it is unlikely the XAFS linear combination can confuse oxides with sulphides. The presence of oxides in the early stage of the corrosion process is also confirmed for natural corrosion of Ag925 [27].

- **Surface state 3 (Fig. 7a, 9 and 15 minutes):** The transformation of the yellow surface state 2 to the blue surface state 3 seems to correspond by the formation of CuS and a decrease in Cu_2S. This means that the colour change might not only be explained by interference of thin films but also by a different mixture of corrosion products in this film.
- **Surface state 4 and 5 (Fig. 7a, 30, 60 and 300 minutes):** The fraction of CuS seems to increase at the expense of Cu_2S, Cu_2O and CuO. At an exposure of 300 minutes, Cu_2O reappeared in larger amounts.

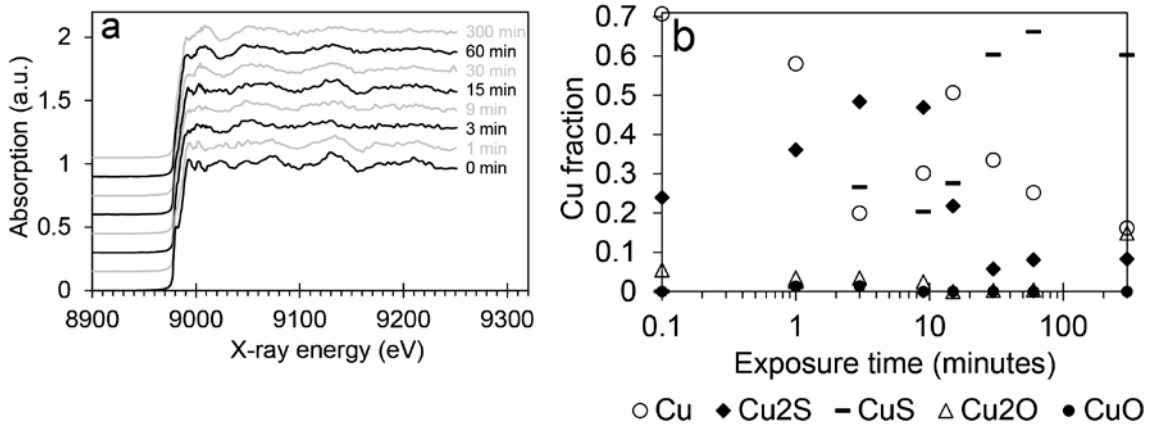

Fig. 7: Surface speciation of a series Ag925 coupons with various exposure times a) XANES spectra of the Cu-K edge c; b) Relative amounts of copper corrosion products as determined by linear combination fitting of the complete spectra shown in fig. 7a.

3.3. In depth characterization of the Ag925 coupon after 60 minutes of exposure

To go further in the analysis of the corrosion layer, a detailed characterization is performed of an Ag925 coupon with an exposure time of 60 minutes. The secondary electron images of Fig. 8 show the presence of spots containing platelets. The tilted SEI image clearly shows that they are considerably higher than the surrounding surface. In Fig. 8b a bump can be seen between the spots containing platelets. The backscattered electron image of the same surface (Fig. 5) shows large dark spots (i.e., bumps or areas rich in platelets). In Fig. 8b, the corrosion layer between the spots appear to be rather rough, although the BSE images in Fig. 5 suggest that this corrosion layer is extremely thin because the underlying Cu-rich inclusions remained visible as small black dots.

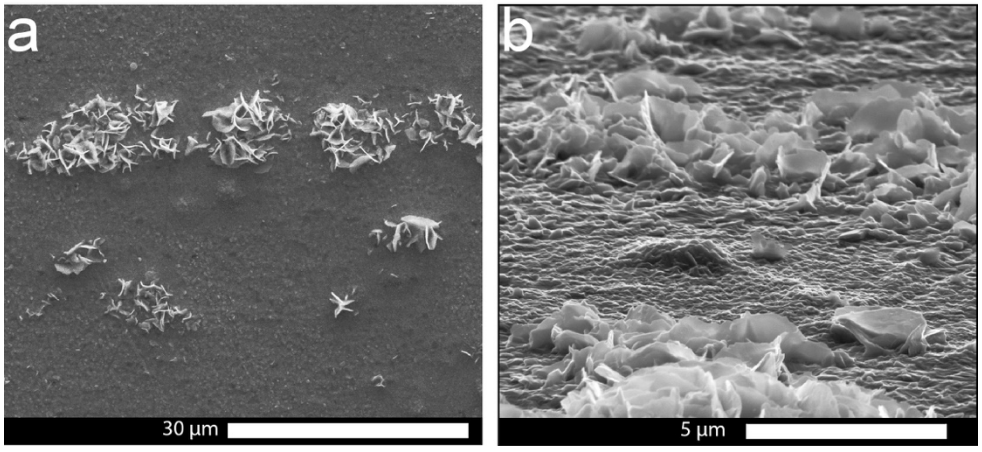

Fig. 8: Morphology of Ag925 exposed for 60 minutes to a sulphide solution as visualized by secondary electron imaging. a) Surface shows spots consisting of platelets; b) Surface is tilted by 75° and shows the presence of spots containing platelets and bumps

The backscattered electron image in Fig. 9 shows the presence of spots containing platelets and small black spots (i.e., Cu-rich inclusions below the corrosion layer). The corresponding X-ray maps clearly demonstrates that all the large spots seen in the BSE image are rich in O, S and Cu. This confirms that

the spots shown in Figs. 2 and 5 must consist of Cu-rich corrosion products. The X-ray map of oxygen suggest the presence of oxides in these spots. This corresponds with the XAFS measurements where oxides reappeared at longer exposure times (see Fig. 7b). Due to a lack of resolution the small spots cannot be visualized in the X-ray maps.

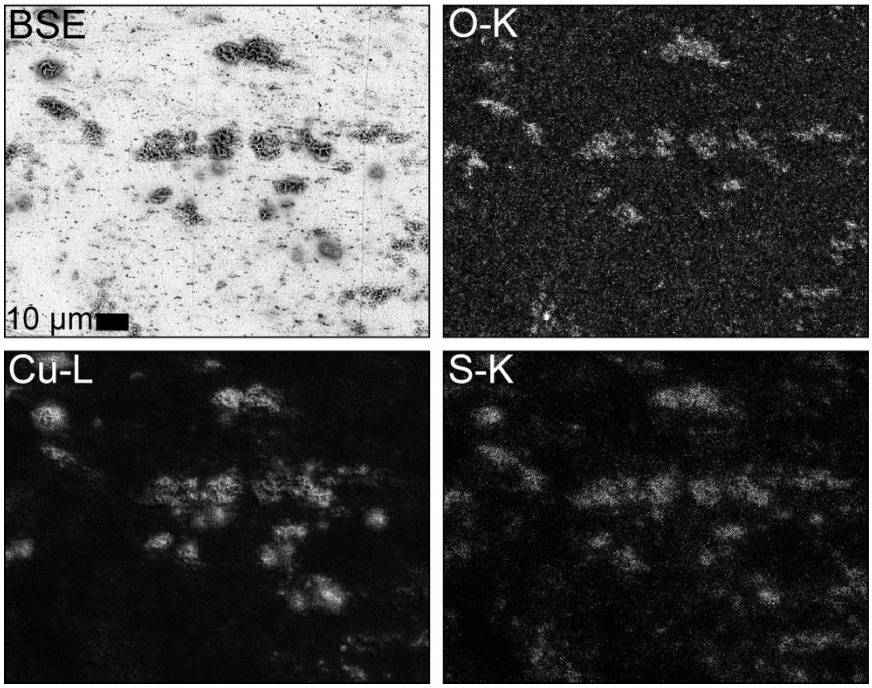

Fig. 9: Backscattered electron image of the surface shown in Fig. 8 and the corresponding X-ray maps showing the distribution of O, Cu and S over the surface. The images are collected at collected at 20 kV and a magnification of 2500x. The dark spots in the backscattered electron images correspond with the zones rich in Cu, S and O.

The analyses in Figs. 2, 5 and 9 show that the corrosion layer is heterogeneous at the µm-level. For a better understanding of this heterogeneity, the top surface (first few nm) is analysed with high resolution XPS at the ELETTRA synchrotron beamline. Fig. 10 shows 2 PEEM images at different kinetic energies suggesting a heterogeneous microstructure of the surface. Three different locations with different aspects are selected for XPS analysis (see circles in Fig. 10b). The XPS spectra of Ag3d, S2p and Cu2p of point 1 show intense lines, but from a chemical point of view this point is similar to points 2 and 3. The analyses suggest the presence of Ag and S with only small amounts of Cu. At the same time, no S-O bonds are detected. This suggests that the Cu-rich bumps and spots containing platelets that can be seen in Figs. 11 and 12 must be covered by a thin Ag_2S-layer of at least a few nm.

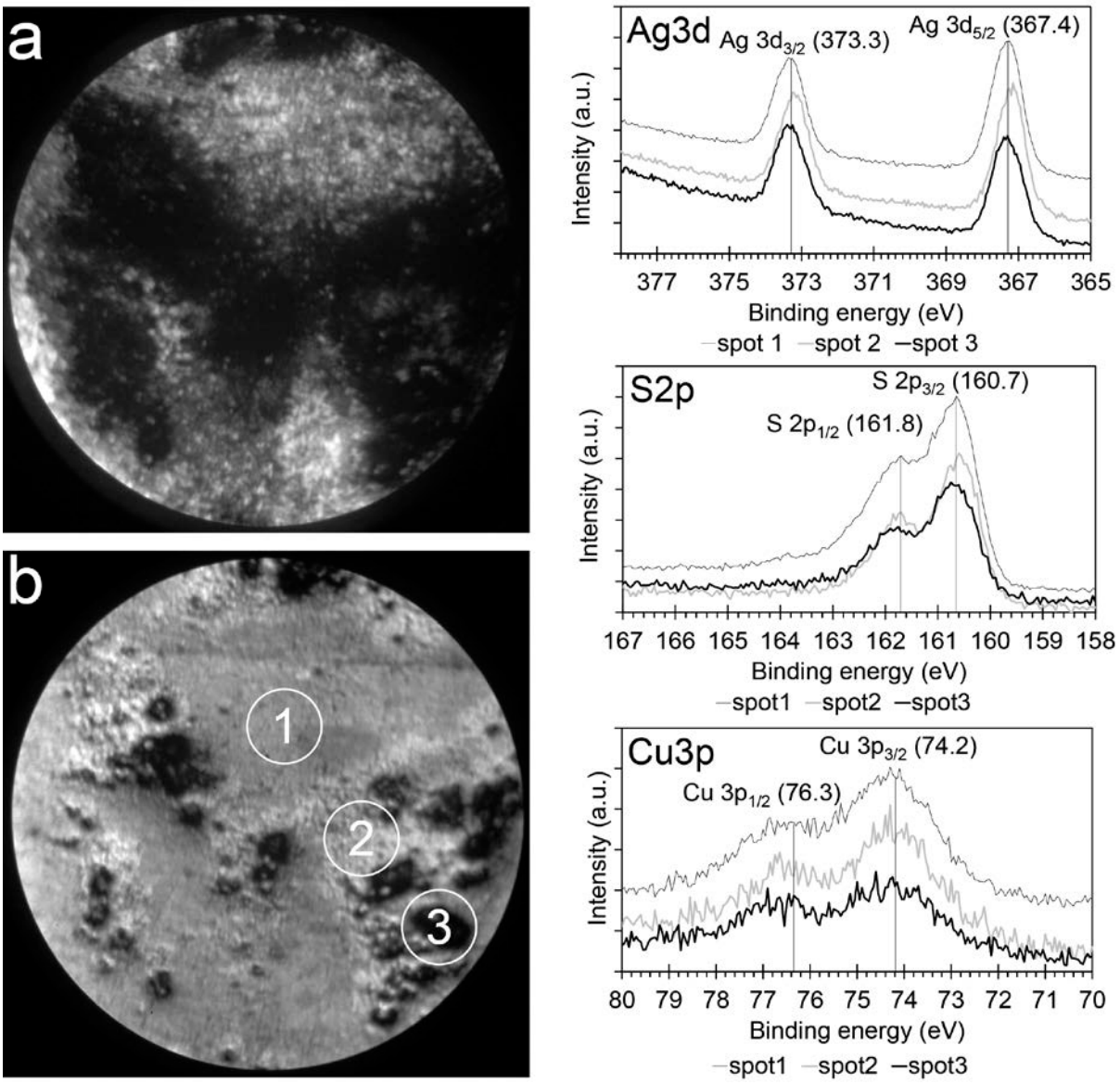

Fig. 10: PEEM images of sulphidized Ag925 with a field of view of 90 µm collected at 2 different energies and high resolution spectra of Ag3d, S2p and Cu3p using a soft X-ray excitation of 450 eV collected at 3 different points. a) Image collected with 3.8 eV electrons. b) Image collected at 4.15 eV and the 3 spots of 13 µm diameter where XPS spectra are collected.

The bright field TEM image in Fig. 11a shows that the corrosion layer of Ag925 with an exposure time of 60 minutes is polycrystalline without any amorphous regions. The grains vary in size (i.e., usually smaller than 200 nm) and are quasi polyhedral. There is no preferential orientation of the grains. The corrosion layer must be considered as a polycrystalline but compact layer of grains without any porosity. The grain from Fig 11b can be indexed with reflection (200) and (220) from the [001] zone of a tetragonal crystal of jalpaite. This indicates that the copper corrosion products formed in an early state must be transformed in a later state in copper-silver corrosion products because silver is only oxidized after some delay. As shown in Fig. 11c, in many grains defects such as twinning are present. Both selected area electron diffraction pattern and HRTEM images reveal that the corrosion layer consists mainly of the jalpaite phase (Ag_3CuS_2) (see Fig 11c-d).

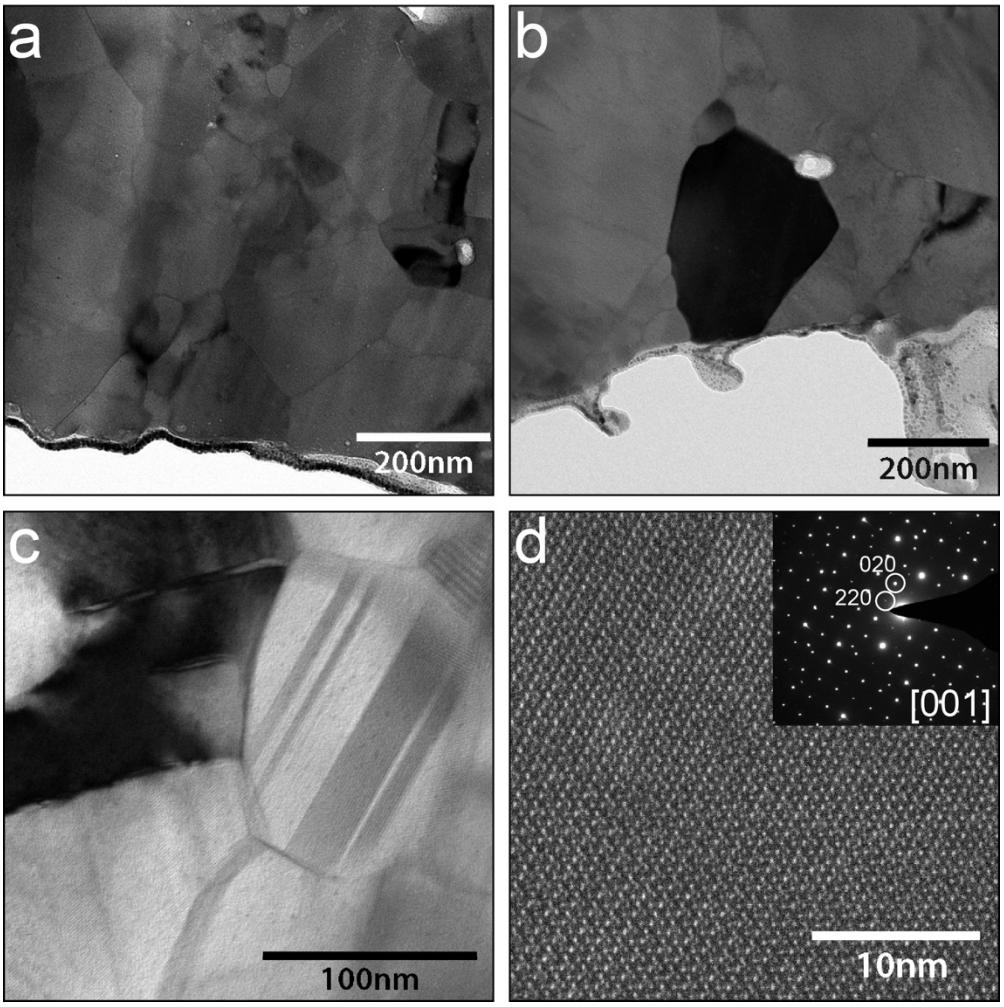

Fig. 11: TEM images from a lamella removed from the corrosion layer of Ag925 with an exposure time of 60 minutes. a) Bright field TEM image showing that the corrosion layer consists of crystalline grains of different sizes; b) Detail of corrosion layer where the black particle is orientated parallel in the direction of the electron beam while all the other particles had another orientation; c) Overview of some grains with twinning defects; d) HRTEM with FFT of the jalpaite phase from the black grain in image b.

The TEM images in Fig. 12 demonstrate the presence at least two different phases. As seen in Fig. 12a and the corresponding X-ray maps, at the boundaries of the jalpaite grain segregation of Ag can be found. In addition, fig. 12b demonstrates the presence of a sulphide rich grain rich in Ag but poor in Cu. This means that the corrosion layer consists of jalpaite grains with Ag_2S segregations or inclusions. The XPS analyses demonstrated that the surface of the corrosion layer is rich in Ag and S but poor in Cu while the powder XRD analysis in Fig. 13 of the scraped-off corrosion layer confirmed the simultaneous presence of jalpaite, acanthite (Ag_2S). This suggests the presence of a thin layer of Ag_2S on the surface of the corrosion layer.

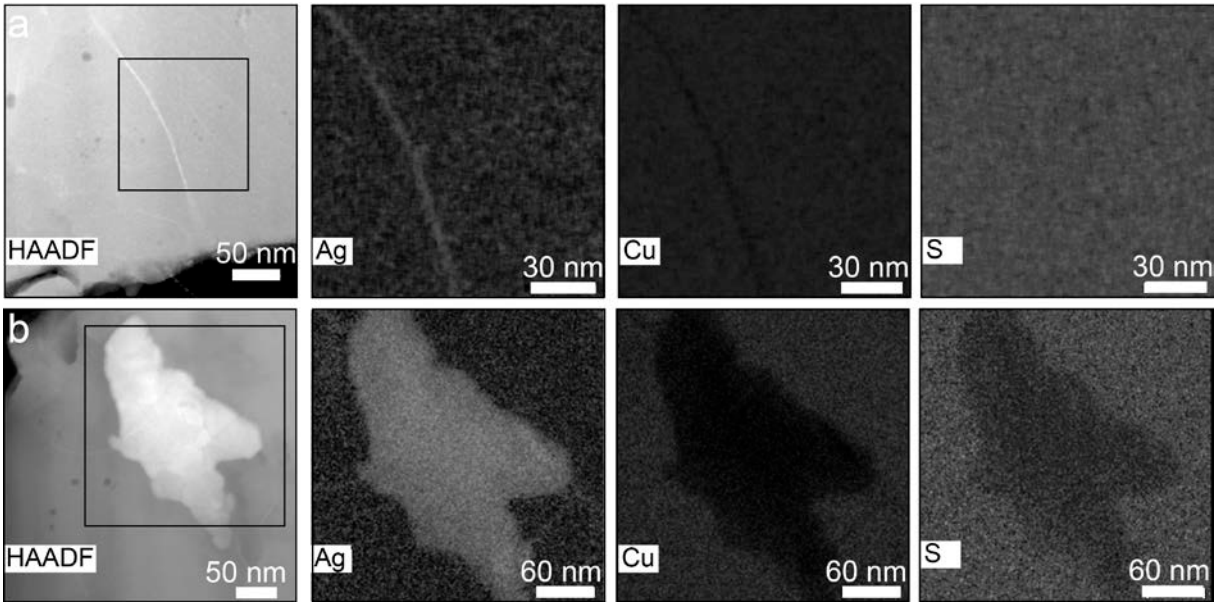

Fig. 12: a) HAADF-STEM image showing the contrast in atomic number at the grain boundary, the HAADF-STEM-EDX maps of the marked area showing the higher Ag concentration at that boundary and the corresponding lower Cu concentration; b) HAADF-STEM image of a grain with a higher average atomic number. The HAADF-STEM-EDX Ag and Cu maps of the marked area shows a higher Ag concentration compared to the surrounding corrosion layer and the absence of Cu in that specific grain.

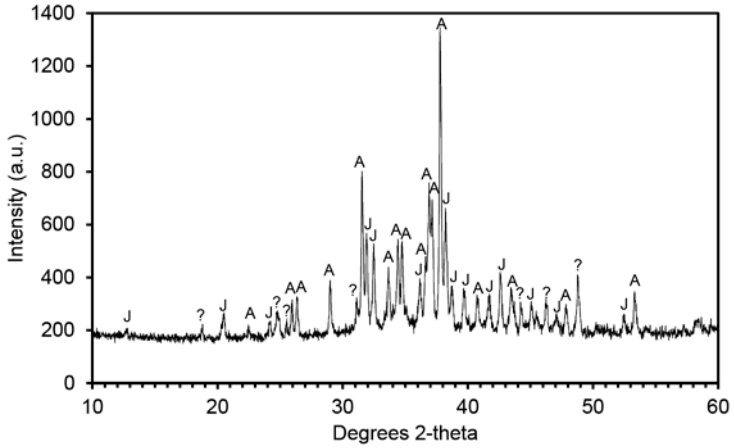

Fig. 13: XRD analysis of corrosion product that scraped off from extensive corrosion of Ag925. The symbols stand for jalpaite (J) and acanthite (A), the question mark for an unidentified crystalline compound.

4. Discussion

The study of the natural corrosion process is hampered by its slow progress and by the uncontrolled and unreproducible corrosion conditions. Therefore, we have chosen to study the corrosion process of an artificial corrosion process to guarantee the reproducibility of this study. We are well aware that artificial corrosion might be governed by a corrosion process that is different from the corrosion in natural conditions. Nevertheless, the study of artificial corrosion gives a good insight in what might occur during natural corrosion. The corrosion of sterling silver by sulphide solutions is accompanied by a change in colour, from white over yellow, over blue until it becomes grey-black. The change in the so-called 'interference colours' are usually explained by the thickening of the tarnish film [3,29,44-46]. However, for Ag925 the difference in light absorption due to the continuous transformation of corrosion products (i.e., chemical colour) can also affect the sequence of colours. In addition, the uniform colour seen at the macroscopic level is composed of zones with different colours at the microscopic level. From the analysed surface properties, it is possible to describe the corrosion process as a sequence of 5 remarkable surface states and transformations between these surface states, which are described below. This description is inspired on the work of Dori [47,48]. The schematic evolution

of Ag925 during the corrosion process is shown in Fig. 14. Results from Fig. 3 indicate that the thickness of the corrosion layer grows fast in the early stage and that it grows slower when corrosion proceeds. Fig. 2 shows that the life-time of the first surface states is shorter than surface state 4 or 5, meaning that also the transformation of the corrosion layer is faster at the beginning of the process.

- **Surface state 1, mirror-like appearance:** At a macroscopic level, the surface has a mirror-like appearance. At a microscopic level, scratches can be seen as a consequence of polishing, as well as Cu-rich inclusions with a diameter of about 1 µm. The distribution of Cu-rich inclusions is not homogeneous and is affected by the production process of the alloy;
- **Transformation from surface state 1 to 2:** The corrosion starts from preferential locations and spots are formed that grow laterally over time. While previously formed spots expand, new spots are formed. The spots have well-defined borders. They are higher in topography and correspond with the bumps and areas containing platelets. From a chemical point of view, there is a preferential oxidation of copper resulting in oxides (i.e., Cu_2O, CuO) and sulphides (i.e., Cu_2S). In this transformation stage, no silver is oxidized.
- **Surface state 2, yellow appearance:** The surface has a yellow appearance at a macroscopic level. However, at a microscopic level the yellow surface is covered by isolated spots. The white spots have a grey centre and blue ring at the border. Since at longer exposure times only the grey coloured centres from these spots remain, these centres can be associated with the presence of platelets. Since these spots are higher in topography compared to the surrounding surface, it explains why the reflectance drops so drastically. The spots must consist of Cu-rich corrosion products because this is the only category of corrosion products that has been identified. The yellow coloured surface between the spots is extremely thin (< 300 nm) because it is transparent in backscattered electron mode.
- **Transformation from surface state 2 to 3:** As corrosion proceeds, the visual appearance of the surface changes from yellow to reddish until a bluish surface is obtained. Only metallic copper is oxidized. As it appears from the redox potential scale, copper is more susceptible to oxidation than silver. It seems that as long as metallic copper is in contact with the surface, copper will oxidize and silver will remain stable. This explains the copper enrichment on the surface.
- **Surface state 3, blue coloured surface:** At a microscopic level, the blue surface is covered by white spots with substantial grey centres consisting of platelets. The thickness of the corrosion layer between the spots remains smaller than 300 nm. At that stage, only the copper undergoes oxidation. Therefore, the spots are still composed of Cu-rich corrosion products.
- **Transformation from surface state 3 to 4:** The reflectance starts to increase again, suggesting that the surface roughness become smoother. The grey centres of the spots become larger while the white zones around these centres expand until they converge into one layer. The blue colour gradually disappears. The Cu-rich inclusions just beneath the surface are emptied, while the Cu-rich spots on the surface further expanded up to 25 µm. The migration of copper at the µm-level occurs in a matter of minutes suggesting a high ionic mobility of copper during the corrosion process. Since the oxidation process and the formation of corrosion products occurs at different locations and because the corrosion process seems to be controlled by the spots, the spots appear to act as fast transport channels [49].
- **Surface state 4, grey surface:** There is still a clear contrast between the dark grey centres and the bright grey surface in between the spots. The Cu-rich inclusions just beneath the surface have clearly been displaced and as a result empty voids remain. The preferential corrosion of copper results in a silver enrichment beneath the corrosion layer. State 4 is still dominated by the selective corrosion of copper, meaning that the colour of surface states 2, 3 and 4 must be caused by the copper corrosion products.
- **Transformation from state 4 to 5:** It is only from surface state 4 onwards that metallic silver starts to oxidize. A solid state reaction occurs in which the previously formed copper sulphide

compounds are transformed into jalpaite (Ag_3CuS_2). From all the Ag-Cu-S compounds (e.g., jalpaite, mckinstryite ($Ag_5Cu_3S_4$), stromeyerite (AgCuS)), jalpaite is the one with the highest amount of silver in its structure. Once it is not possible anymore to incorporate oxidized silver in the Ag-Cu-S compounds, acanthite (Ag_2S) is formed at the jalpaite grain boundaries. Due to the displacement of silver, the voids beneath the corrosion layer become substantially larger.

- **Surface state 5, dark grey surface:** At the microscopic level, the corrosion layer is very heterogeneous. In light microscopy, the contrast between the grey centres and the surface between the spots starts to diminish. However, in backscattered electron mode the spots remain clearly visible and have well-defined borders. The spots are rich in Cu and S but the presence of O reappeared. At a nm-level, the corrosion layer consists of jalpaite grains with random orientation containing twinning defects. In addition, Ag_2S can be found inside the corrosion layer at the jalpaite grain boundaries or as small grains between the jalpaite grains but also as a thin film on top of the corrosion layer. Due to this thin film, surface analytical techniques with a depth resolution in the µm range (i.e., FEG-ESEM-EDX) suggest that the corrosion layer is heterogeneous while techniques with a depth resolution in the nm-scale (i.e., SR-XPS) suggest that the corrosion layer is homogeneous and rich in Ag and S but poor in Cu.
- **Further transformation:** Although the results in this article are limited to Ag 925 enduring a specific accelerated corrosion process, they might shed some light on the natural corrosion of Ag-Cu alloys. At 300 minutes of exposure time, the voids become so large that the attachment of the corrosion layer to the substrate is almost completely lost. This might explain why corrosion layers exfoliate when they reach a critical thickness as is observed by others [49]. In these studies, corrosion layers with a thickness up to 14 µm have been observed for extended corrosion of silver-copper alloys. Others report the existence of a multi-layered system with Cu-rich corrosion layer sandwiched between an Ag-rich corrosion layer and the alloy [50-52]. This extended surface state is not observed here, but it seems a logic extrapolation of the corrosion process studied in this investigation.

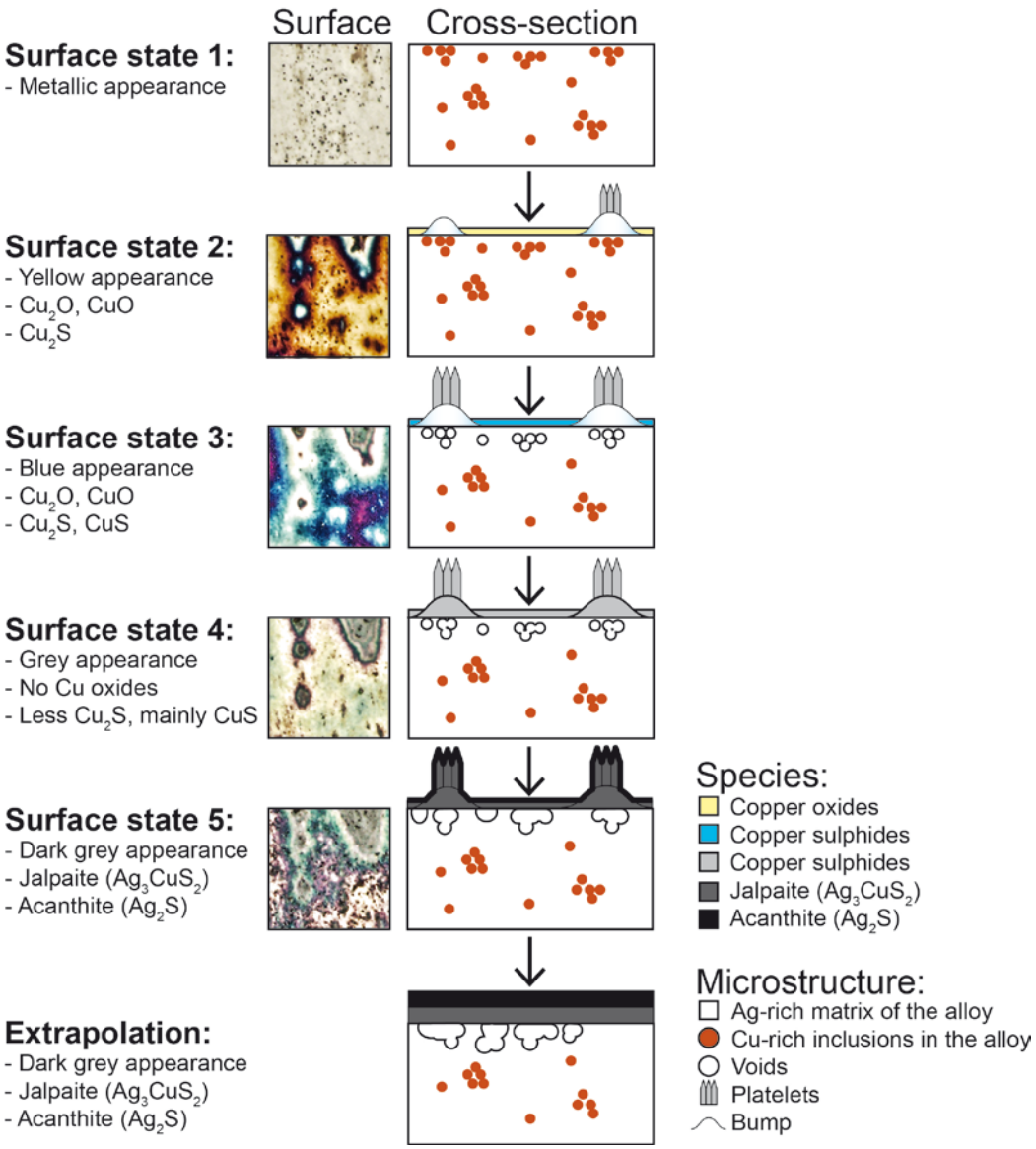

Fig. 14: Evolution of the Ag925 surface during the corrosion process. The main surface states are visualized with microscopic images of the surface and with schematic cross sections. The arrows represent the transformations between the surface states.

5. Conclusions

This investigation illustrates the complexity of the corrosion process of a sterling silver-copper alloy exposed to a Na_2S solution. The small copper amounts in sterling silver dramatically changes the corrosion process of the alloy compared to pure silver. The thickness of the corrosion layer grows fast in the beginning of the process. At the same time, the chemical composition, the mixture of corrosion products and the microstructure of the interface between corrosion layer and bulk metal evolves fast as well. As corrosion proceeds, the increase in thickness and the evolution of the corrosion layer slows down. Based on all these transformations, the corrosion process of Ag925 is described by a series of 5 subsequent surface states, although continuous transitions exist between these surface states. After 300 minutes of exposure, the corrosion layer has a thickness of about 1 µm. The most remarkable conclusions concerning the corrosion process are summarized in the list below.

- Copper is preferentially oxidized due to a difference in redox potential scale between copper and silver. As a consequence, an accumulation of copper occurs at the surface;
- Due to the displacement of copper from the metal towards the surface, a silver enrichment below the corrosion layer occurs. This means that the chemical composition of the alloy just beneath the corrosion layer changes over time.

- During the corrosion process, the microstructure of the interface changes considerably. The Cu-rich inclusions just beneath the surface are transformed into voids. When metallic silver starts to oxidize, the voids become substantially larger so that the attachment of the corrosion layer to the metal below is weakened. The solid state reactions occur very fast because both Cu and Ag are able to migrate over distances of several µm in a matter of minutes.
- It is important to realize that the mixture of corrosion products evolves as corrosion proceeds. Several corrosion products are formed after another and some of these corrosion products formed in an earlier state are transformed into other products. Therefore, the species present in the corrosion layer have a limited life-time;
- The yellow, blue and grey surface states at the beginning of the corrosion process are dominated by copper corrosion products. Only in surface state 5, the oxidation of silver played a major role resulting in the transformation of Cu-rich corrosion products into Ag-Cu-S corrosion products. Although the colour of corrosion layer is usually explained by interference of thin films, it may also be explained by the sequence of copper corrosion products formed after another;
- Only in surface state 5, jalpaite (Ag_3CuS_2) has been identified as a major corrosion product but it is covered by a thin film of acanthite (Ag_2S). It explains why micro-analytical techniques observed a heterogeneous corrosion layer and XPS a homogeneous corrosion layer.

Acknowledgements
The authors are grateful for the financial support by the EU-FP7 grant PANNA no. 282998 and for the opportunity to perform SR-XPS measurements at the NanoESCA beamline of the Elettra storage ring, under the approval of the advisory Committee (Proposal No. 20135164), as well as the opportunity to perform XANES measurements at the DUBBLE beamline of the ESRF storage ring (Proposal no. 26-01-990). The authors are grateful for the financial support by the STIMPRO project FFB150215 of the University of Antwerp. Pieter Tack is funded by a Ph.D. grant of the Agency for Innovation by Science and Technology (IWT). We would also like to thank Peter Van den Haute for the XRD measurements that were performed at the University of Ghent.

References
[1] D. A. Scott, Ancient Metals: Microstructure and Metallurgy: Volume 1.Copper and copper alloys (Conservation Science Press, Los Angeles, 2012) pp. 44-69

[2] L. Selwyn, Metals and Corrosion: A handbook for the conservation professional (Canadian Conservation Institute, Ottawa, 2004) pp. 131-140

[3] V. Costa, Rev. Conserv. **2**, 19 (2001)

[4] J.D. Sinclair, J. Electrochem. Soc. **129(1)**, 33-40 (1982)

[5] T.E. Graedel, J.P. Franey, G.J. Gualtieri, G.W. Kammlott, D.L. Malm, Corros. Sci. **25(12)**, 1163 (1985)

[6] H.A. Ankersmit, N.H. Tennent, S.F. Watts, Atmos. Environ. **39**, 695 (2005)

[7] ASHRAE, in *2011 ASHRAE handbook: Heating, ventilating, and air-conditioning applications* (SI edition, American Society of Heating, Refrigerating and Air-conditioning Engineers, 2011) pp. 23.1-23.23.

[8] M. Watanabe, S. Shinozaki, E. Toyoda, K. Asakura, T. Ichino, N. Kuwaki, Y. Higashi, T. Tanaka, Corrosion **62(3)**, 243 (2006)

[9] T.E. Graedel, J. Elecrochem. Soc. **139(7)**, 1963 (1992)

[10] J.P. Franey, G.W. Kammlott, T.E. Graedel, Corros. Sci. **25(2)**, 133 (1985)

[11] J.P. Franey, Corros. Sci. **23(3)**, 1 (1983)

[12] H. Kim, Mater. Corros. **54**, 243 (2003).

[13] Ch. Kleber, R. Wiesinger, J. Schnöller, U. Hilfrich, H. Hutter, M. Schreiner, Corros. Sci. **50**, 1112 (2008)

[14] R. Wiesinger, J. Schnöller, H. Hutter, M. Schreiner, Ch. Kleber, Open Corr. J. **2**, 96 (2009)

[15] R. Wiesinger, M. Schreiner, Ch. Kleber, Appl. Surf. Sci. **256**, 2735 (2010)

[16] M.C. Bernard, E. Dauvergne, M. Evesque, M. Keddam, H. Takenouti, Corr. Sci. **47**, 663 (2005)

[17] J.I. Lee, S. M. Howard, J.J. Kellar, W. Cross, K.N. Han, Metall. Mater. Trans. B **32B**, 895 (2001)

[18] G.W. Vinal, G.N. Schramm, Metal Ind. **22(1)**, 15 (1924)

[19] A. Lins, N. McMahon, in *Thirteenth international symposium on the conservation and restoration of cultural property*, 4-6 October 1989 (Tokyo, Japan) pp. 135-162.

[20] M.G. Dowsett, A. Adriaens, M. Soares, H. Wouters, V.V.N. Palitsin, R. Gibbons, R.J.H. Morris, Nucl. Instrum. Methods Phys. Res., Sect. B **239**, 51-64 (2005)

[21] I.D. MacLeod, Stud. Conserv. **36(4)**, 222-234 (1991)

[22] S. Capelo, P. M. Homem, J. Cavalheiro, I. T. E. Fonseca, J. Solid State Electrochem. **17**, 223– 234 (2013)

[23] N. Salvado, S. Buti, A. Labrador, G. Cinque, H. Emerich, T. Pradell, Anal. Bioanal. Chem. **399**, 3041–3052 (2011)

[24] C.J. Raub, R.D. Blumer, in *Metal95: Proceedings of the international conference on metals conservation*, Semur-en-Auxois, France, 25-28 September 1995 (James and James, London, 1997), pp. 67-70.

[25] G.M. Ingo, S. Balbi, T. De Caro, I. Fragala, E. Angelini, G. Bultrini, Appl. Phys. A **83**, 493–497 (2006)

[26] E. Angelini, T. de Caro, A. Mezzi, C. Riccucci, F. Faraldi, S. Grassini, Surf. Interface Anal. **44**, 947-952 (2012)

[27] P. Storme, O. Schalm, R. Wiesinger, Herit. Sci. **3(25)**, (2015) doi:10.1186/s40494-015-0054-1

[28] W. Van Laer, Weg-Wyzer voor aankoomende Gouden Zilversmeeden (In Dutch) (Amsterdam, 1725, reprinted by De Tijdstroom, Lochem, 1967)

[29] J. Hammes, Goud Zilver Edelstenen (in Dutch) (De Technische Boekhandel H. Stam, Amsterdam, 1943)

[30] G. Wharton, S.L. Maish, W.S. Ginell, JAIC, **29(1)**, 13-32 (1990)

[31] Norm NBN EN ISO 8891:2000

[32] CIE DS 014-4.3/E:2007

[33] ASTM standard B825-02

[34] H. Sone, T. Tamura, K. Miyazaki, S. Hosaka, Microelectron. Eng., **83(4-9)**, 1487-1490 (2006)

[35] M. Dapor, Monte Carlo simulation of backscattered electrons and energy from thick targets and surface films, Phys. Rev. B **46(2)**, 619-625 (1992)

[36] Anderson C.A., Hasler M.F., in X-ray Optics and Microanalysis, Fourth International Congress on X-ray Optics and Microanalysis, Orsay, 1965, R. Castaing, P. Deschamps, K. Philibert Eds., Herman, Paris, 1966, p. 310

[37] S. Nikitenko, A. M. Beale, A. M. van der Eerden, S. D. Jacques, O. Leynaud, M. G. O'Brien, D. Detollenaere, R. Kaptein, B. M. Weckhuysen, W. J. Bras, Synchrotron Radiat. **15**, 632-640 (2008)

[38] S. Bals, W. Tirry, R. Geurts, Z. Yang, D. Schryvers, Microsc. Microanal., **13(2)**, 80-86 (2007)

[39] D.M. Trots, A. Senyshyn, D.A. Mikhailova, T. Vad, H. Fuess, J. Phys. Condens. Matter. **20(45)**, 455204 (2008)

[40] O. Schalm, P. Storme, Microsc. Anal. **20**, 10-15 (2015)

[41] S. Licht, J. Electrochem. Soc. **135(12)**, 2971-2975 (1988)

[42] T.T.M. Tran, C. Fiaud, E.M.M. Sutter, A. Villanova, Corr. Sci. **45**, 2787-2802 (2003)

[43] T.T.M. Tran, C. Fiaud, E.M.M. Sutter, Corr. Sci. **47**, 1724–1737 (2005)

[44] A. Kutzelnigg, , Kolloid Z. **61**, 48-50 (1932)

[45] M.S. Barger, W.B. White, The daguerreotype: nineteenth-century technology and modern science, (Smithsonian Institution, Washington, 1991) p. 162

[46] H.A. Ankersmit, A. Domenech Carbo, N.H. Tennent, in *Metal 2001: Proceedings of the ICOM Committee for Conservation Metals Working Group* (2001) pp. 157-166.

[47] J. Somekh, M. Choder, D. Dori, M. Choder, PLoS ONE, **7(12)**, e51430 (2012)

[48] J. Somekh, G. Haimovich, A. Guterman, D. Dori, M., Choder, PloS ONE, **9(9)**, e107085 (2014)

[49] J.H. Payer, G. Ball, B.I. Rickett, H.S. Kim, Mater. Sci. Eng., A **198**, 91-102 (1995)

[50] R. Van Langh, H.A. Ankersmit, I. Joosten, in *Proceedings of Metal 2004,* 4–8 October 2004 (National Museum of Australia Canberra ACT) pp. 137-141

[51] R. Linke, M. Schreiner, G. Demortier, M. Alram, X-ray spectrom., **32**, 373-380 (2003)

[52] R. Linke, M. Schreiner, G. Demortier, Nucl. Instrum. Methods Phys. Res., Sect. B **226**, 172–178 (2004)